Supplementary Information:

Molecular basis for inhibition of AcrB multidrug efflux pump by novel and powerful pyranopyridine derivatives

Hanno Sjuts[1], Attilio V. Vargiu[2*], Steven M. Kwasny[3], Son T. Nguyen[3], Hong-Suk Kim[4], Xiaoyuan Ding[3], Alina R. Ornik[1], Paolo Ruggerone[2], Terry L. Bowlin[3], Hiroshi Nikaido[4*], Klaas M. Pos[1*], Timothy J. Opperman[3*]

[1]Institute of Biochemistry, Goethe Universität Frankfurt, Max-von-Laue-Straße 9, D-60438 Frankfurt, Germany
[2]Department of Physics, University of Cagliari, S.P. Monserrato-Sestu Km 0.700, I-09042 Monserrato (CA), Italy
[3]Microbiotix, Inc., One Innovation Dr., Worcester, MA 01605 USA
[4]University of California Berkeley, 16 Barker Hall # 3202, Berkeley, CA 94720-3202 USA
*Corresponding author. E-mail: topperman@microbiotix.com (T.J.O.); pos@em.uni-frankfurt.de (K.M.P.); vargiu@dsf.unica.it (A.V.V.); nhiroshi@berkeley.edu (H.N.)

Materials and Methods:

Bacterial strains, growth media, and reagents.
The bacterial strains that were used in this study are listed in Extended Data Table 6. Luria Broth (Miller) and agar were purchased as prepared dehydrated media from Becton Dickenson (Franklin Lakes, NJ). Ciprofloxacin (CIP) was purchased from ICN Biomedicals (Aurora, OH). Hoechst 33342 (H33342) was purchased from Molecular Probes (Eugene, OR). The following reagents were purchased from Sigma Aldrich (St. Louis, MO): levofloxacin (LVX), piperacillin (PIP), tazobactam, minocycline (MIN), nitrocefin. The pyranopyridine efflux pump inhibitors (MBX2319, MBX2931, MBX3132 and MBX3135) were synthesized as described (1).

Antibacterial assays.
Assays to measure the Minimum Inhibitory Concentration (MIC) of antibacterial agents were performed as described in the CLSI guidelines (CLSI 2006) with modifications described previously (2). Checkerboard assays measuring the minimal concentration of an Efflux Pump Inhibitor (EPI) required to decrease the MIC of an antibiotic by 4-fold (MPC4) and time kill assays were conducted as described (2).

Efflux assays.
The H33342 accumulation assay was used to evaluate the effect of EPIs on the activity of the AcrAB-TolC efflux pump in several bacterial species essentially as described(3). The effects of EPIs on the kinetic parameters of nitrocefin efflux catalyzed by AcrAB-TolC in *E. coli* were estimated using the β-lactamase assay(4).

AcrBper cloning.
Two independent PCR reactions were performed to amplify the coding regions for the N- and C-terminal periplasmic loop regions Ala39-Thr329 and Ser561-Ser869, respectively, from a plasmid containing the wild-type *acrB* gene as template, using the primers

AcrBper1_f: 5'-ATATAT*GCTCTTC*T*AGT**GCACCGCCGGCAGTAACG**-3';
AcrBper1_r: 5'-GGATCC**GCCTGAACCGCC****GGTGTCGTATGGGTAAAC**-3';
AcrBper2_f: 5'-GGATCC**GGCGGTTCA****AGCTCCTTCTTGCCAGATG**-3';
AcrBper2_r: 5'-TATATA*GCTCTTC*A*TGC**GGAGGAGAGACGTTCCTGATAGG**-3'.

The two PCR products were ligated together *via* the inserted *Bam*HI restriction site (underlined).
This generates a glycine/serine linker (amino acid sequence GGSGGSGGS, nucleotides belonging to the glycine/serine linker are shown in bold) connecting both periplasmic loops (bold underlined nuclecotides belong to *acrB*). The fragment exchange (FX) cloning technique was conducted to insert the ligated PCR product into the cloning vector pINITIAL using the *Sap*I restriction enzyme (5). The *Sap*I recognition site is shown in italics and its cleavage site is indicated with an asterisk. The sequence-verified *acrBper* DNA was subcloned *via* the FX cloning technique into the expression vector pBXCPD (a kind gift from Emanuele Marine, Goethe University Frankfurt), containing an arabinose inducible promoter. AcrBper is expressed covalently fused to a Cysteine Protease Domain (CPD), and a C-terminal His_{10} tag. The protease activity of the CPD is highly specific for its N-terminal A-L-A-

D-G-K sequence and requires the presence of inositol hexakisphosphate (IP6) for protease activity. Upon addition of IP6, the CPD autocatalytically removes itself and the His_{10} tag by proteolytic cleavage of the the L-A peptide bond (6).

AcrBper expression.

E. coli MC1061 cells were transformed with the pBXCPD::*acrBper* plasmid and plated on LB-agar supplemented with 100 µg/ml ampicillin. A single colony was used to inoculate an overnight starting culture, which was incubated at 37 °C while rigorously shaking. The overnight culture was used to inoculate (1:500 dilution) the main culture (one liter of 2x YT, supplemented with ampicillin), which was grown at 37 °C, 110 rpm until an OD_{600} of 0.8 was reached. Protein overexpression was induced by adding 0.002 % (w/v) L-arabinose (Roth) and cells were grown for additional four hours at 37°C. Cells were harvested by centrifugation (6,000 rpm, 15 minutes) and stored at -20°C until use.

AcrBper purification.

Cell pellets were resuspended in buffer A (50 mM HEPES, pH 7, 300 mM NaCl; 5 $ml \times g^{-1}$ wet weight), supplemented with phenylmethylsulfonylfluoride (PMSF; 0.1 mM), DNase (10 µg/ml) and lysozyme (10 µg/ml; all from Sigma) and stirred on ice for 30 minutes. Cells were lysed by a single passage through an automated cell disruptor at 20 kPsi and non-soluble material was removed by centrifugation (30,000 rpm, Beckman 45Ti rotor, 45 minutes, 4 °C). All purification steps were performed at 4 °C. Imidazole (15 mM final concentration; Sigma) was added to the supernatant and loaded onto a NiNTA agarose (Qiagen) column (bed volume 1.5 ml), pre-equilibrated with buffer A containing 15 mM imidazole. After washing the column with buffer A containing first 30 mM imidazole (15 column volumes) and then without imidazole (15 column volumes), CPD-mediated cleavage between AcrBper and CPD-His_{10} was initiated by the addition of 15 ml buffer A supplemented with 150 µM IP6. The cleavage reaction was conducted for 16 hours at mild sample agitation. Liberated AcrBper was collected in the flow-through fraction and concentrated using a 30 kDa cut-off Amicon spin concentrator centrifuged at 4,000 rpm. Size-exclusion chromatography on a Superdex 200 column (GE Healthcare) equilibrated with buffer B (10 mM HEPES, pH 7, 150 mM NaCl) was used as final purification step of AcrBper. Overexpression and purification of DARPin clone 1108_19 was done as previously described(7) except for the final purification step of the DARPin's, which was done using a Superdex 200 column and buffer B (see above) as running buffer.

Crystallization.

Crystallization trials of AcrBper were set up at 18 °C using vapor diffusion techniques. Drops contained 1.5 µl of AcrBper/DARPin solution (equimolar ratio, 13.5 mg/ml total protein concentration) and 1.5 µl of precipitant solution over 800 µl precipitant solution in the reservoir well. Rod shaped crystals were obtained using 0.1 M MES pH6.5, 0.21 M NaCl, 11.5 % PEG 4000 as reservoir solution and reached maximum size within 10 - 14 days.

Soaking of AcrBper crystals with MBX inhibitors.

All MBX compounds were dissolved in DMSO to a final concentration of 50 mM. These stock solutions were diluted to 1 mM with the reservoir solution that yielded crystals of AcrBper. Crystals were transferred into these solutions and incubated for 24 - 72 hours as hanging drops over reservoir solution. Afterwards, the crystals were

briefly soaked in a solution composed of reservoir solution supplemented with 15 % PEG 300 as cryoprotectant, before they were looped, flash-cooled and stored in liquid nitrogen until measured.

Soaking of AcrBper crystals with Minocycline and Rhodamine 6G (R6G).
Minocycline (20 mM, Sigma) and R6G (10 mM, AppliChem) were prepared in 10 mM HEPES, pH 7, 150 mM NaCl. These stocks were diluted to a 10 mM minocycline and a 5 mM R6G soaking solution with the reservoir solution used for crystallization. AcrBper crystals were soaked in these solutions for one week, prior to cryoprotection as described above.

Structure determination.
Crystals were measured on the beamlines, PXIII (Swiss Light Source, Villigen, Switzerland) and PX1 (Synchrotron SOLEIL, Paris, France) and P13 (Deutsches Elektronen Synchrotron, Hamburg, Germany). All datasets were reduced and scaled using XDS(8). Crystals belong to space group $P2_12_12_1$ with approximate unit cell dimensions of a = 108 Å; b = 145 Å; c = 174 Å. The apo structure of AcrBper was solved by molecular replacement using PHASER(9) with wild-type AcrB and DARPin coordinates from the pdb entry 4DX5 as a search model, omitting all atom coordinates that are not part of AcrBper. The model was improved by iterative cycles of manual model building in Coot (10) and restrained refinement using REFMAC5 (11). Phases of the ligand bound structures were derived from rigid body refinements (REFMAC5) using the final model of the AcrBper/DARPin *apo* coordinates as an input model and were completed using Coot and REFMAC5 as described above. Coordinate and restrained definition files for the MBX compounds were generated using JLIGAND from the CCP4 suite (12). Data collection and refinement statistics are summarized in Extended Data Table 4. The structure figures were prepared with PyMOL (www.pymol.org).

Molecular dynamics simulations.
Force field parameters for MBX2319 were taken from previous published work (13), and are now publicly available at the link: http://www.dsf.unica.it/translocation/db (14). The parameters for the remaining inhibitors MBX2931, MBX3132 and MBX3135 were generated following previously published protocol (15). Namely, the Marvin package [Marvin 6.2.0, 2014, ChemAxon (http://www.chemaxon.com)] was used to calculate the most likely protonation states of the inhibitors at pH 7.0; all of them turned out to be neutral in these conditions. The force field parameters were taken from the GAFF force field (16), and the AMBER14 package (17). Atomic Restrained Electrostatic Potential (RESP) charges were derived using the antechamber tool of AMBER, after a structural optimization performed with Gaussian09 (18) in the presence of implicit solvent (PCM).
Four simulations (one for each complex) each of 20 ns in length were performed in the presence of explicit water solution (0.1 M KCl) using the program AMBER14. The TIP3P model of water(19) and the monovalent ion parameters appropriate for this choice were used(20). A time step of 2 fs was used. Pressure and temperature were regulated at 1 atm and 310 K (after the equilibration phase) using the isotropic Berendsen barostat(21) and the Langevin thermostat(22), respectively. Periodic boundary conditions were employed. Electrostatic interactions were evaluated using the Particle Mesh Ewald scheme with a cutoff of 9.0 Å for the short-range evaluation

in direct space. The same cutoff was used for Lennard-Jones interactions (with a continuum model correction for energy and pressure).

In order to guarantee a slow equilibration phase while keeping the asymmetric structure of AcrBper in accordance to the crystallographic data, the equilibration and the production runs were performed as followed: In order to rearrange the position of waters and ions, structural relaxation was performed in the presence of soft restraints (1 kcal·mol^{-1}·Å^{-2}) on all the non-hydrogen atoms of the protein and the ligand. In the second and third steps, the restraints were kept only on backbone and C_α atoms, respectively, and on the non-hydrogen atoms of ligand. Finally, restraints were removed from the ligand and from a selection of residues having at least one atom within 8 Å from the ligand. In all steps the structure of the solute from the previous step was used as target for restraints, and up to 10,000 optimization steps were performed using the conjugate-gradients algorithm. Next, annealing up to 340 K was performed in 2 ns, using the same setup as in the last step of the relaxation described at the previous point, and constant volume and temperature conditions (NVT ensemble). This was followed by quenching to 310 K in 3 ns, and then a 1 ns long equilibration with same setup as above, but in the NTP ensemble. Finally, a productive run of 20 ns in length was performed applying partial restraints to the system, namely to all heavy atoms of the protein but those having at least one atom within 8 Å from the ligand. The last conformation from previous dynamics was used as target for structural restraints. The trajectories were saved every 20 ps, resulting in ~2000 conformations for each system.

Post-processing of trajectories. The free energy of binding of each inhibitor to AcrB was evaluated using the Molecular Mechanics – Generalized Born Surface Area (MM-GBSA) post-processing method, through the MMPBSA.py tool of the AmberTools package(23).

According to the MM-GBSA theory, the free energy of binding ΔG_b is evaluated through the following formula:

$$\Delta G_b = G_{com} - \left(G_{rec} + G_{lig}\right)$$

where G_{com}, G_{rec}, and G_{lig} are the absolute free energies of complex, receptor, and ligand, respectively, averaged over the equilibrium trajectory of the complex (single trajectory approach(24–26). According to these schemes, the free energy difference can be decomposed as:

$$\Delta G_b = \Delta E_{MM} + \Delta G_{solv} - T\Delta S_{conf}$$

where ΔE_{MM} is the difference in the molecular mechanics energy, ΔG_{solv} is the solvation free energy, and $T\Delta S_{conf}$ is the solute conformational entropy. The first two terms were calculated with the following equations:

$$\Delta E_{MM} = \Delta E_{bond} + \Delta E_{angle} + \Delta E_{torsion} + \Delta E_{vdw} + \Delta E_{elec}$$
$$\Delta G_{solv} = \Delta G_{solv,p} + \Delta G_{solv,np}$$

E_{MM} includes the molecular mechanics energy contributed by the bonded (E_{bond}, E_{angle}, and $E_{torsion}$) and non-bonded (E_{vdw} and E_{ele}, calculated with no cutoff) terms of the force field. ΔG_{solv} is the solvation free energy, which can be modeled as the sum of an electrostatic contribution ($\Delta G_{solv,p}$, evaluated using the MM-GBSA approach)

and a non-polar one ($\Delta G_{solv,np} = \gamma \Delta S_A + b$, proportional to the difference in solvent-exposed surface area, ΔS_A).

In the MM-GBSA approach, the electrostatic solvation free energy was calculated using the implicit solvent model developed in Ref. *48* (igb = 8 in AMBER14) in combination with mbondi3 (28, 29) (for H, C, N, O, S elements) and intrinsic (30) radii. Partial charges were taken from the AMBER/GAFF force fields, and relative dielectric constants of 1 for solute and 78.4 for the solvent (0.1 M KCl water solution) were used. The non-polar contribution is approximated by the LCPO (31) method implemented within the sander module of AMBER. In addition to being faster, the MM-GBSA approach furnishes an intrinsically easy way of decomposing the free energy of binding into contributions from single atoms and residues (32), which is alternative to the “alanine scanning” approach.

Solvation free energies were calculated on ~300 frames, extracted from the production trajectories. The solute conformational entropy contribution ($T\Delta S_{conf}$) was not included in the evaluation of the free energy(26).

Root Mean Square Fluctuation (RMSF) values were calculated through the cpptraj module of the AMBER14 package, and temperature factors B were calculated from the RMSF values using the formula:

$$B = \frac{8}{3}\pi^2 (RMSF)^2$$

The analyses as well as the atomic-level figures, were performed using tcl scripts within VMD (33) or utilities of the AMBER package.

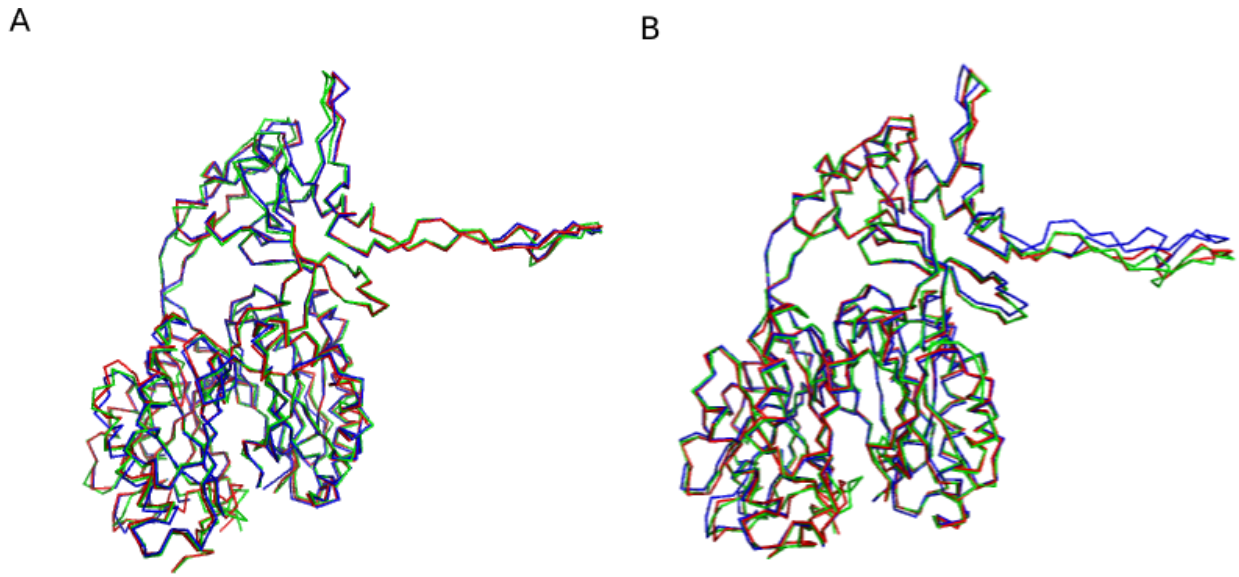

Fig. S1. Superimposition between AcrBper and the periplasmic domains of the full-length AcrB crystal forms. A) Overlay of the Loose protomers with AcrBper (chain A) in blue, AcrB (pdb entry 4DX5, chain A, (34)) in red and AcrB (pdb entry 2GIF, chain C, (35)) in green. B) Superimposition of the respective Tight protomer periplasmic domains using the same color coding as in A).

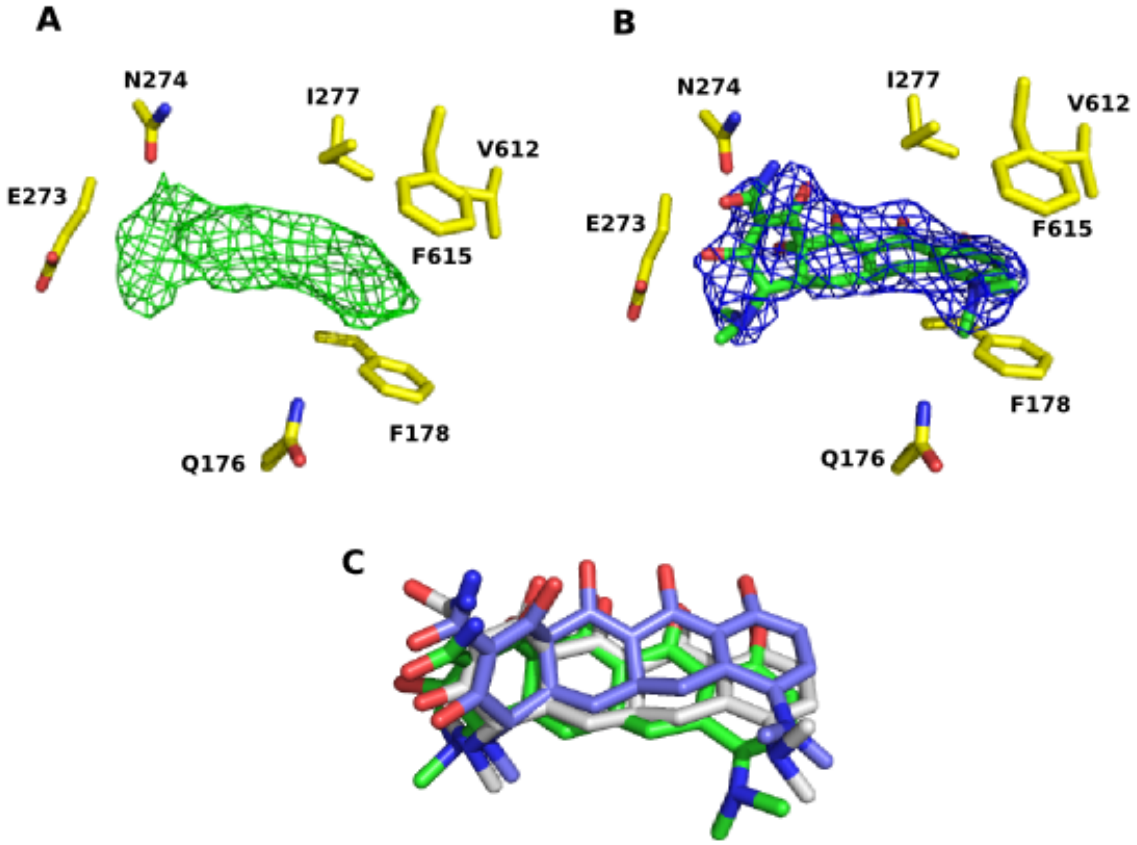

Fig. S2. Minocycline (MIN) binding to the deep binding pocket of the AcrB T monomer. A) The F_o-F_c omit map of MIN is shown as green mesh, contoured at 3.0σ. B) The blue mesh (contoured at 1.0σ) represents the MIN 2F_o-F_c density after refinement of the complex structure. Side chain residues of the AcrB deep binding pocket are shown as sticks (carbon = yellow; oxygen = red; nitrogen = blue). C) Superimposition of MIN coordinates as bound to the AcrB deep binding pocket. The MIN atom positions were extracted from pdb entry 4DX5 (carbon = light blue; oxygen = red; nitrogen= blue(34)); pdb entry 2DRD (carbon = gray; oxygen = red; nitrogen = blue(35)); the AcrBper/MIN complex (carbon = green; oxygen = red; nitrogen = blue; this study).

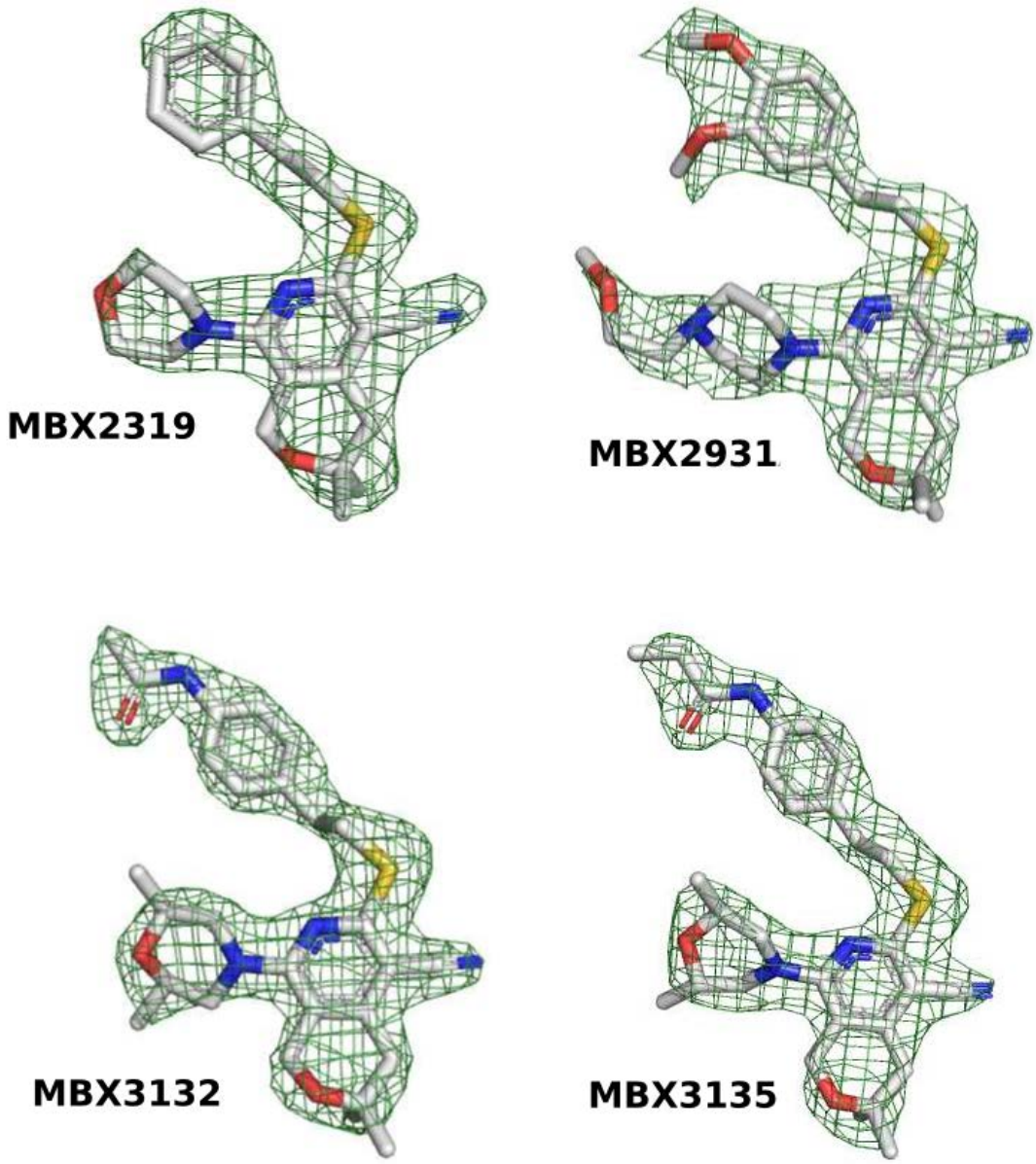

Fig. S3. **Residual positive electron density of MBX2319, MBX2931, MBX3132 and MBX3135.** The omit F_o-F_c maps are contoured at 2.5σ, 3.0σ, 4.0σ and 4.0σ for MBX2319, MBX2931, MBX3132 and MBX3135, respectively. The assigned MBX compounds are shown as sticks (carbon = gray; oxygen = red; nitrogen = blue; sulfur = yellow).

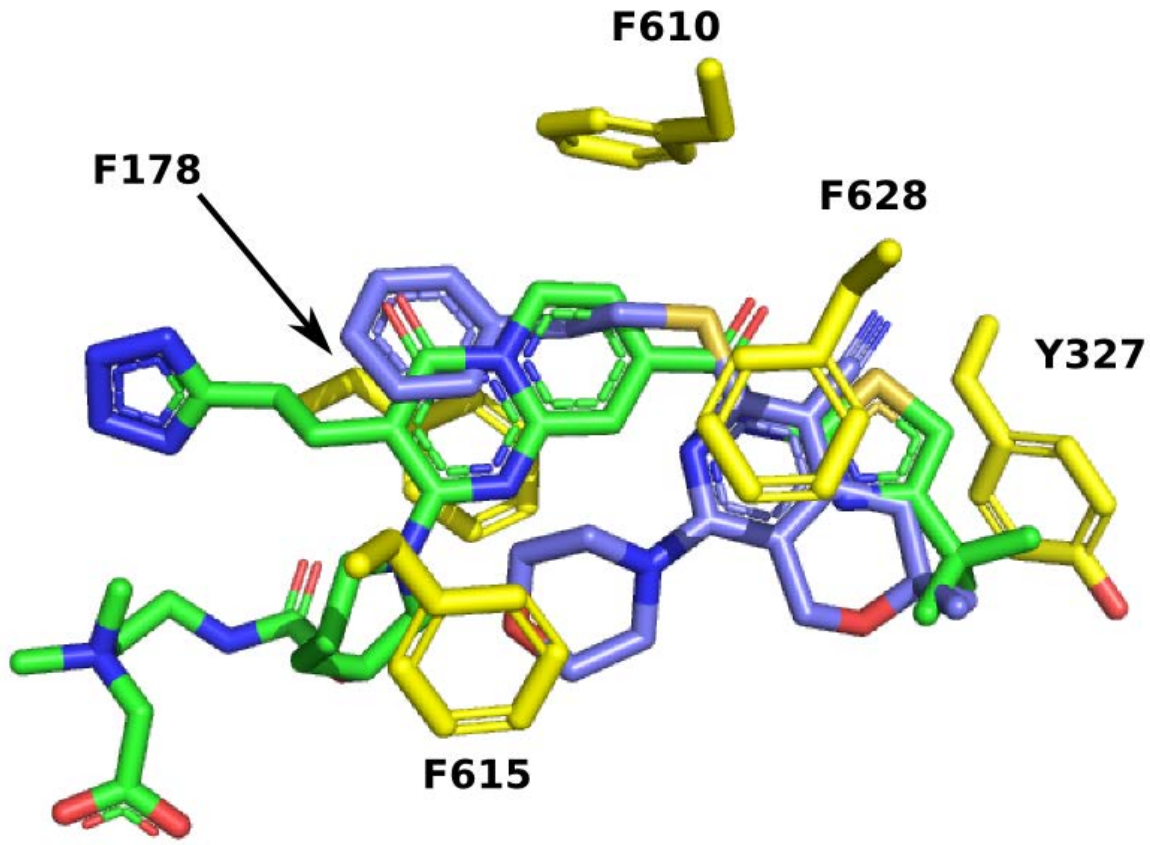

Fig. S4. Superimposition of MBX2319 and D13-9001 inhibitors bound to AcrB. MBX2319 (carbon = light blue; oxygen = red; nitrogen = blue; sulfur = yellow) and D13-9001 (carbon = green; oxygen = red; nitrogen = blue; sulfur = yellow; pdb entry 3W9H(36)) bind in the deep binding pocket and associated hydrophobic trap of AcrB. Protein side chains are shown as sticks (carbon = yellow; oxygen = red).

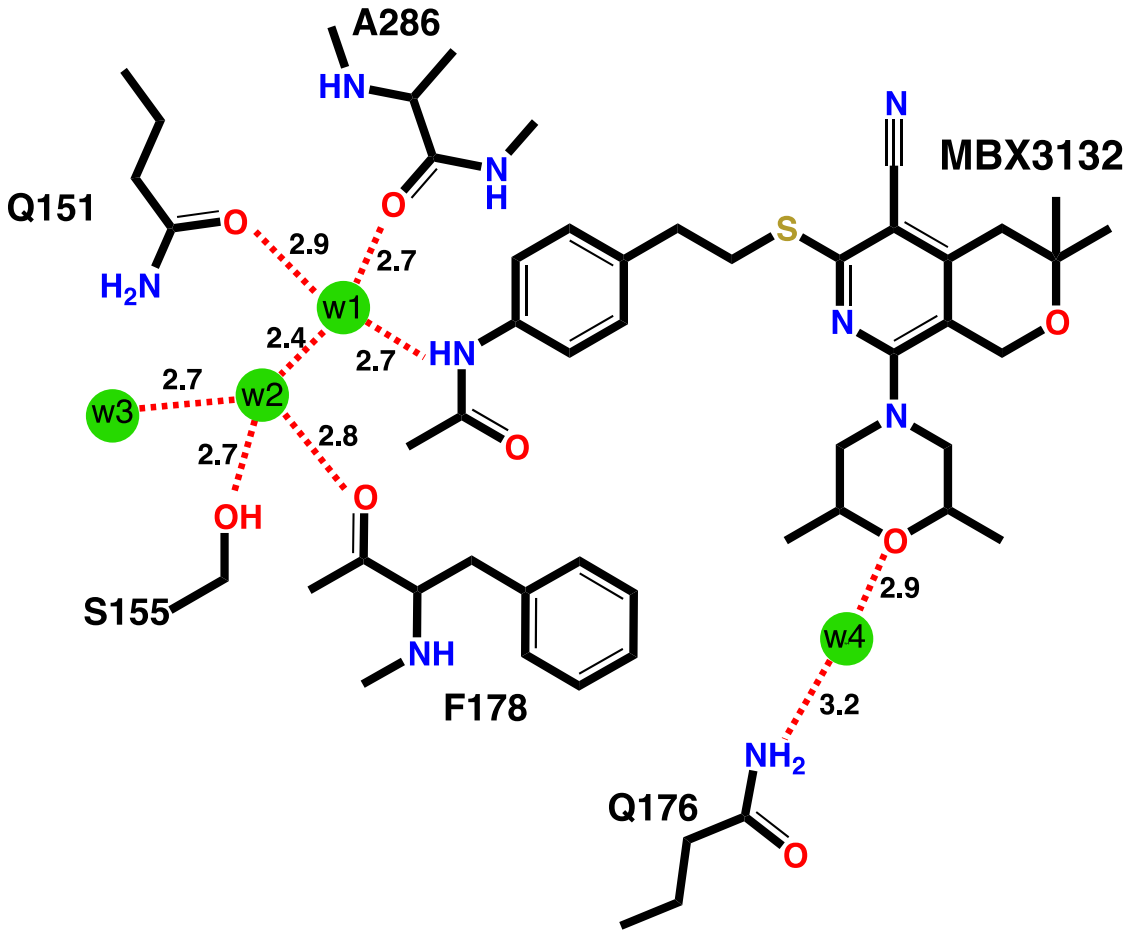

Fig. S5. Schematic illustration of the water-mediated hydrogen bond network between MBX3132 and AcrB. Waters are shown as green circles. Hydrogen bonds are indicated by red dotted lines with distances given in Å.

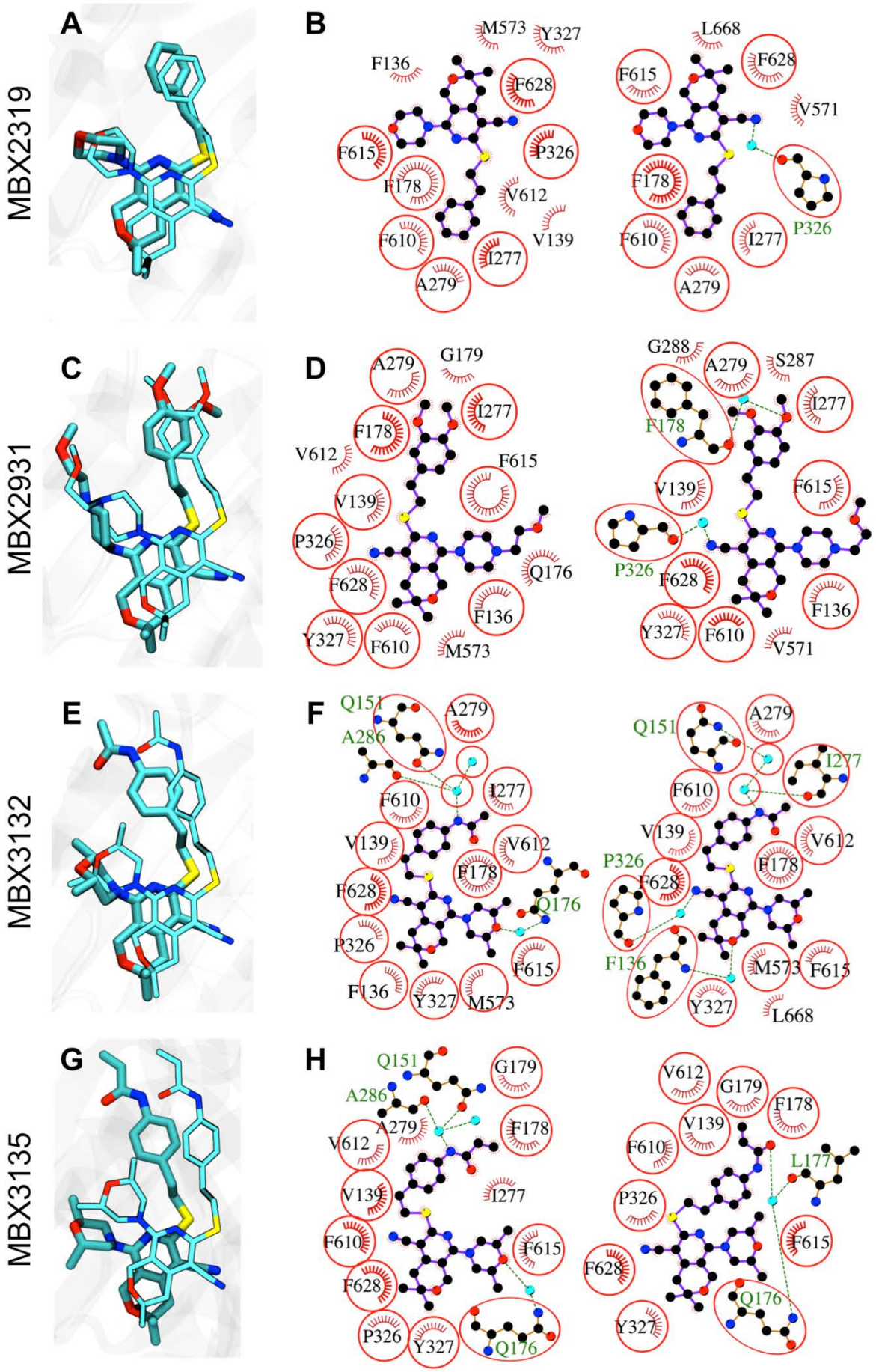
MBX2319
A
B
M573
Y327
F136
F628
F615
P326
F178
V612
V139
F610
I277
A279
L668
F628
F615
V571
F178
P326
F610
I277
A279
MBX2931
C
D
A279
G179
I277
F178
V612
F615
V139
P326
Q176
F628
F136
Y327
F610
M573
G288
A279
S287
I277
F178
V139
F615
P326
F628
F136
Y327
F610
V571
MBX3132
E
F
Q151
A279
A286
I277
F610
V139
V612
F178
F628
Q176
P326
F615
F136
Y327
M573
Q151
A279
I277
F610
V139
V612
P326
F178
F628
F136
M573
F615
Y327
L668
MBX3135
G
H
Q151
G179
A286
A279
F178
V612
I277
V139
F610
F615
F628
P326
Y327
Q176
V612
G179
F178
V139
F610
L177
P326
F615
F628
Q176
Y327

290

Fig. S6. Comparison between crystal structures determined by X-ray diffraction and most representative conformations extracted from partly restrained MD simulations. A, C, E, G) Comparison between X-ray and MD structures for compounds MBX2319, MBX2931, MBX3132 and MBX3135. X-ray and MD-derived structures are shown with thinner and thicker sticks respectively (carbon = cyan; oxygen = red; nitrogen = blue, sulfur = yellow). The RMSD values between X-ray and MD derived positions are 1.2, 1.8, 1.6 and 1.4 Å, respectively. B, D, F, H) Comparison of interactions between the four MBX compounds and residues at the AcrB deep binding pocket as represented by LigPlot+ on the X-ray- (left panel) and MD-derived (right panel) structures. Residues involved in MBX binding as derived from both techniques are highlighted by red circles.

Table S1. **RMSD values between protomers after Cα-atom alignment.** Indicated in bold are the lowest RMSD values of the AcrBper protomers with the AcrB L and T protomers derived from the periplasmic domains from the full-length structures 4DX5 and 2GIF.

Crystal		AcrBper $P2_12_12_1$ PDB 5EN5			AcrB $P2_12_12_1$ PDB 4DX5			AcrB C2 PDB 2GIF		
	Monomer	L chain A	L chain B	T chain C	L chain A	T chain B	O chain C	L chain A	T chain B	O chain C
AcrBper $P2_12_12_1$ PDB 5EN5 DARPin bound	L chain A	0	0.242	0.869	**0.355**	1.237	1.379	**0.537**	1.228	1.690
	L chain B		0	0.589	**0.547**	1.193	1.366	**0.626**	1.116	1.708
	T chain C			0	1.131	**0.692**	2.150	0.991	**0.659**	2.056
AcrB $P2_12_12_1$ PDB 4DX5 DARPin bound	L chain A				0	2.084	2.021	0.556	2.064	2.143
	T chain B					0	2.039	1.783	0.486	2.036
	O chain C						0	1.809	1.989	0.440
AcrB C2 PDB 2GIF DARPin free	L chain A							0	1.706	1.835
	T chain B								0	1.856
	O chain C									0

Table S2. The spectrum of efflux pump inhibitor activity of MBX2319 and selected analogs against representative pathogenic *Enterobacteriaceae*.

		MIC	MPC4 (μM) for MBX#:			
Organism	Drug	(μg/ml)	**2319**	**2931**	**3132**	**3135**
Escherichia coli	LVX	0.06	3.12	12.5	≤ 0.19	≤ 0.19
ATCC 700928	TZP	2	≥ 12.5	0.78	0.78	0.39
	MIN	1	3.12	12.5	≤ 0.19	≤ 0.19
E. coli	LVX	32	≥ 12.5	0.78	0.39	0.39
331	TZP	4	1.56	1.56	≤ 0.19	≤ 0.19
	MIN	32	3.12	3.12	≤ 0.19	≤ 0.19
Shigella flexneri	LVX	0.06	6.25	≥ 25	≤ 0.19	≤ 0.19
ATCC 700930	TZP	0.5	≥ 12.5	12.5	0.78	0.39
	MIN	1	6.25	3.12	0.78	≤ 0.19
Salmonella enterica	LVX	0.63	≥ 12.5	1.56	0.39	≤ 0.19
MDCH06	TZP	4	6.25	12.5	≤ 0.19	≤ 0.19
	MIN	8	3.12	3.1	≤ 0.19	≤ 0.19
Enterobacter aerogenes	LVX	0.06	≥ 25	3.1	1.56	≤ 0.39
ATCC 13048	TZP	8	≥ 25	≥ 25	≥ 25	≥ 25
	MIN	8	1.56	0.78	≤ 0.39	≤ 0.39
Klebsiella pneumoniae	LVX	1	6.25	3.12	3.12	≤ 0.39
ATCC 700603	TZP	40	≥ 25	≥ 25	≥ 25	≥ 25
	MIN	64	6.25	1.56	≤ 0.39	≤ 0.39

Abbreviations: LVX, levofloxacin; TZP, piperacillin + tazobactam (8:1 ratio); MIN, minocycline; MIC, minimal inhibitory concentration; MPC4, minimum potentiation concentration of the MBX compound that decreases the MIC of the antibiotic by 4-fold.

Table S3. **Crystallographic data collection and refinement statistics.** Values in parentheses are for the highest resolution shell.

	Apo	MBX2319	MBX2931	MBX3132	MBX3135	Rhodamine 6G	Minocycline
pdb entry	5EN5	5ENO	5ENP	5ENQ	5ENR	5ENS	5ENT
Data collection							
Beamline	SLS, PXIII	SLS, PXIII	Soleil, PX1	Soleil, PX1	SLS, PXIII	SLS, PXIII	DESY, P13
Wavelength (Å)	1.0000	0.97794	0.97857	0.97857	1.0000	1.0000	0.97625
Temperature (K)	100	100	100	100	100	100	100
Resolution range (Å)	50.0-2.3 (2.44-2.30)	50.0-2.2 (2.33-2.20)	50.0-1.9 (2.01-1.90)	50.0-1.8 (1.91-1.80)	50.0-2.3 (2.44-2.30)	50.0-2.8 (2.97-2.80)	50.0-2.5 (2.59-2.50)
Space group	$P2_12_12_1$	$P2_12_12_1$	$P2_12_12_1$	$P2_12_12_1$	$P2_12_12_1$	$P2_12_12_1$	$P2_12_12_1$
Unit cell a, b, c (Å)	108.29, 145.24, 174.37	108.76, 145.15, 174.24	108.65, 145.34, 174.22	107.73, 145.52, 173.45	109.07, 145.49, 174.24	108.65, 145.24, 174.15	109.56, 145.41, 175.61
Total reflections	839239	1914247	1755111	2264342	843941	460613	87165
Unique reflections	122373	140556	216569	251472	122939	68419	96991
Multiplicity	6.9 (6.8)	13.6 (12.2)	8.1 (7.9)	9.0 (8.7)	6.9 (7.0)	6.7 (6.6)	9.0 (8.9)
Completeness (%)[a)]	99.3 (98.1)	99.7 (98.5)	99.6 (98.1)	99.8 (99.0)	99.7 (99.3)	99.7 (98.9)	99.3 (99.3)
Mean I / σ(I)	6.75 (1.31)	5.27 (0.92)	9.34 (1.08)	12.96 (1.08)	5.96 (1.32)	5.16 (1.19)	11.50 (1.45)
R_{merge} (%)	19.1 (121.2)	30.7 (163.0)	11.6 (143.8)	10.6 (194.9)	22.4 (122.3)	28.5 (127.3)	16.2 (124.1)
R_{meas} (%)	20.6 (121.2)	32.0 (158.7)	12.3 (137.4)	11.2 (179.0)	24.2 (122.9)	30.9 (130.1)	57.3 (131.8)
Wilson B-factor (Å^2)	30.15	27.03	29.86	30.55	26.34	38.82	44.9
CC1/2 (%)[a)]	98.7 (46.2)	98.4 (47.3)	99.7 (46.0)	99.9 (48.4)	98.0 (44.5)	95.8 (41.9)	99.7 (61.7)
Refinement							
Resolution range (Å)	50.0-2.3 (2.44-2.30)	50.0-2.2 (2.33-2.20)	50.0-1.9 (2.01-1.90)	50.0-1.8 (1.91-1.80)	50.0-2.3 (2.44-2.30)	50.0-2.8 (2.97-2.80)	50.0-2.5 (2.59-2.50)
R_{work}	0.1966 (0.2824)	0.1991 (0.2793)	0.1817 (0.3123)	0.1819 (0.3217)	0.1935 (0.2772)	0.1948 (0.2935)	0.1950 (0.3146)
R_{free}[b)]	0.2486 (0.3300)	0.2464 (0.3287)	0.2215 (0.3253)	0.2229 (0.3328)	0.2401 (0.3152)	0.2564 (0.3374)	0.2559 (0.3600)
No. of non-H atoms	17497	17885	18212	18265	17713	17010	17298
Macromolecules	16904	16871	16893	16875	16876	16724	16886
Ligand	-	29	37	35	36	33	40
Water	593	985	1282	1355	801	253	372
Average B factor (Å^2)							
All atoms	36.2	32.7	35.0	37.0	32.0	42.9	52.3
Macromolecule	36.6	33.0	35.0	36.9	32.4	43.2	52.3
Ligand	-	52.4	52.2	29.7	27.4	59.7	76.2
Water	26.3	26.6	34.9	38.4	24.4	22.7	37.4
Ramachandran favored (%)	96	97	97	97	97	97	96
Ramachandran outliers (%)	0.14	0.18	0.18	0.14	0.18	0.14	0.27
RMSD, bonds (Å)	0.015	0.016	0.018	0.018	0.016	0.011	0.013
RMSD, angles (°)	1.67	1.72	1.82	1.80	1.72	1.50	1.59
MolProbity[1] clash score (see 37)	1.40	1.22	1.82	1.94	1.25	1.86	1.13

[a)] Criterion for resolution cut-off: CC1/2 > 40%.
[b)] The same set of R_{free} reflections (5% of the apo dataset) was used for all datasets.

Table S4. Differences in the thermodynamics of binding to the deep pocket in AcrBper by MBX2931, MBX3132 and MBX3135 relative to MBX2319. In the second and third column the overall differences in free energies of binding ($\Delta\Delta G_b$) and the differences (in kcal/mol) between the sum of contributions from residues of the deep binding pocket ($\Delta\Delta G_b^{DP}$) are reported, respectively. Cells from the fourth to the last column report the differences in per-residue contributions to ΔG_b, and are colored from red (negative, increased contribution) to blue (positive, decreased contribution). Residues contributing to the binding of all four MBX inhibitors are underlined, and residues comprising the hydrophobic trap (36) are shown in bold. The stabilization due to interaction of MBX compounds with the DP increases in going from MBX2319 to MBX3135. In particular, the weight of the DP goes from ~ 30% with MBX2931 to ~ 60% with MBX3135.

	$\Delta\Delta G_b$	$\Delta\Delta G_b^{DP}$	**F136**	V139	**F178**	I277	A279	S287	P326	Y327	V331	M333	**F610**	V612	**F615**	F617	**F628**
MBX2931	**-5.0**	**-1.6**		0.4		-1.4	0.1		0.4	-0.5	-0.6	0.2	0.1		-1.5	0.8	0.4
MBX3132	**-5.9**	**-3.4**	0.5	0.3	-1.2	-1.5	-0.4	-0.7	0.2	-0.3	-0.1	-0.3		-0.3	0.4		
MBX3135	**-6.9**	**-4.2**	0.2	0.5	-1.7	-1.5	-0.4	-0.8	0.2	-0.5	-0.3	0.2		-0.3	0.4	0.2	-0.4

Table S5. Bacterial strains that were used in this study.

Organism	Strain	Genotype/Description	Source (Ref)
Escherichia coli	AB1157	*thr*-1, *araC14*, *leuB6*(Am), Δ(*gpt-proA*)62, *lacY*1, *tsx*-33, qsr'-0, *glnV*44(AS), *galK*2(Oc), LAM-, Rac-0, *hisG*4(Oc), *rfbC*1, *mgl*-51, *rpoS*396(Am), *rpsL*31(strR), *kdgK*51, *xylA*5, *mtl*-1, *argE*3(Oc), *thi*-1	(38)
Escherichia coli	331	CIP^R, UTI isolate	Baylor College of Medicine
Escherichia coli	ATCC 700928	UTI isolate	ATCC#
Escherichia coli	HN1157	F', *araD*139, ∆(*argF-lac*)U169, *rpsL*150, *rel*-I, *flb*-5301, *pts*F25, *deoC*I, *thi*-J, ∆*lamB*106, ∆*ompF*80, *zei06*::Tn10, *ompC*I24, *acrR*::Kan	(4)
Enterobacter aerogenes	ATCC 13048		ATCC#
Klebsiella pneumoniae	ATCC 700603		ATCC#
Shigella flexneri	ATCC 700930		ATCC#
Salmonella enterica (typhimurium)	MDCH06		BEI Resources
Pseudomonas aeruginosa	ATCC 27853		ATCC#

#ATCC, American Type Culture Collection

References:

1. Nguyen ST, et al. (2015) Structure-activity relationships of a novel pyranopyridine series of Gram-negative bacterial efflux pump inhibitors. *Bioorg Med Chem* 23(9):2024–2034.
2. Opperman TJ, et al. (2014) Characterization of a novel pyranopyridine inhibitor of the AcrAB efflux pump of Escherichia coli. *Antimicrob Agents Chemother* 58(2):722–733.
3. Coldham NG, Webber M, Woodward MJ, Piddock LJ V. (2010) A 96-well plate fluorescence assay for assessment of cellular permeability and active efflux in Salmonella enterica serovar Typhimurium and Escherichia coli. *J Antimicrob Chemother* 65(May):1655–1663.
4. Nagano K, Nikaido H (2009) Kinetic behavior of the major multidrug efflux pump AcrB of Escherichia coli. *Proc Natl Acad Sci U S A* 106(14):5854–5858.
5. Geertsma ER, Dutzler R (2011) A versatile and efficient high-throughput cloning tool for structural biology. *Biochemistry* 50(15):3272–3278.
6. Shen A, et al. (2009) Simplified, enhanced protein purification using an inducible, autoprocessing enzyme tag. *PLoS One* 4(12):e8119.
7. Sennhauser G, Amstutz P, Briand C, Storchenegger O, Grütter MG (2007) Drug export pathway of multidrug exporter AcrB revealed by DARPin inhibitors. *PLoS Biol* 5(1):e7.
8. Kabsch W (2010) XDS. *Acta Crystallogr Sect D Biol Crystallogr*:125–132.
9. McCoy AJ, et al. (2007) Phaser crystallographic software. *J Appl Crystallogr* 40:658–674.
10. Emsley P, Lohkamp B, Scott WG, Cowtan K (2010) Features and development of Coot. *Acta Crystallogr Sect D Biol Crystallogr* 66:486–501.
11. Murshudov GN, et al. (2011) REFMAC5 for the refinement of macromolecular crystal structures. *Acta Crystallogr Sect D Biol Crystallogr* 67:355–367.
12. Lebedev AA, et al. (2012) JLigand: A graphical tool for the CCP4 template-restraint library. *Acta Crystallogr Sect D Biol Crystallogr* 68:431–440.
13. Vargiu A V., Ruggerone P, Opperman TJ, Nguyen ST, Nikaido H (2014) Inhibition of E. coli AcrB multidrug efflux pump by MBX2319: molecular mechanism and comparison with other inhibitors. *Antimicrob Agents Chemother* 58(10):6224–6234.
14. Malloci G, et al. (2015) A Database of Force-Field Parameters, Dynamics, and Properties of Antimicrobial Compounds. *Molecules* 20(8):13997–14021.
15. Vargiu A V., Nikaido H (2012) Multidrug binding properties of the AcrB efflux pump characterized by molecular dynamics simulations. *Proc Natl Acad Sci U S A* 109(50):20637–20642.
16. Wang J, Wolf RM, Caldwell JW, Kollman PA., Case DA. (2004) Development and testing of a general Amber force field. *J Comput Chem* 25(9):1157–1174.
17. Case DA, et al. (2015) AMBER 2015.
18. Frisch MJ, et al. (2009) Gaussian 09, Revision A.1.
19. Jorgensen WL, Chandrasekhar J, Madura JD, Impey RW, Klein ML (1983) Comparison of simple potential functions for simulating liquid water. *J Chem Phys* 79(2):926–935.
20. Joung IS, Cheatham TE (2008) Determination of alkali and halide monovalent ion parameters for use in explicitly solvated biomolecular simulations. *J Phys Chem B* 112(30):9020–9041.
21. Berendsen HJC, Postma JPM, van Gunsteren WF, DiNola A, Haak JR (1984)

Molecular dynamics with coupling to an external bath. *J Chem Phys* 81(8):3684–3690.
22. Feller SE, Zhang Y, Pastor RW, Brooks BR (1995) Constant pressure molecular dynamics simulation: The Langevin piston method. *J Chem Phys* 103(11):4613–4621.
23. Miller BR, et al. (2012) MMPBSA.py: An efficient program for end-state free energy calculations. *J Chem Theory Comput* 8(9):3314–3321.
24. Kollman PA, et al. (2000) Calculating structures and free energies of complex molecules: Combining molecular mechanics and continuum models. *Acc Chem Res* 33(12):889–897.
25. Fogolari F, Brigo A, Molinari H (2002) The Poisson-Boltzmann equation for biomolecular electrostatics: A tool for structural biology. *J Mol Recognit* 15(6):377–392.
26. Genheden S, Ryde U (2015) The MM/PBSA and MM/GBSA methods to estimate ligand-binding affinities. *Expert Opin Drug Discov* 0441(November):1–13.
27. Shang Y, Nguyen H, Wickstrom L, Okur A, Simmerling C (2011) Improving the description of salt bridge strength and geometry in a Generalized Born model. *J Mol Graph Model* 29(5):676–684.
28. Onufriev A, Bashford D, Case DA (2004) Exploring protein native states and large-scale conformational changes with a modified generalized born model. *Proteins Struct Funct Bioinforma* 55(2):383–394.
29. Bondi A (1964) Van der Waals Volumes and Radii. *J Phys Chem* 68(3):441–451.
30. Tsui V, David A, Case DA (2000) Molecular Dynamics Simulations of Nucleic Acids with a Generalized Born Solvation Model. *J Am Chem Soc* 122(11):2489–2498.
31. Weiser J, Shenkin PS, Still WC (1999) Approximate Atomic Surfaces from Linear Combinations of Pairwise. 20(2):217–230.
32. Gohlke H, Kiel C, Case DA (2003) Insights into protein-protein binding by binding free energy calculation and free energy decomposition for the Ras-Raf and Ras-RalGDS complexes. *J Mol Biol* 330(03):891–913.
33. Humphrey W, Dalke A, Schulten K (1996) VMD: Visual molecular dynamics. *J Mol Graph* 14(1):33–38.
34. Eicher T, et al. (2012) Transport of drugs by the multidrug transporter AcrB involves an access and a deep binding pocket that are separated by a switch-loop. *Proc Natl Acad Sci U S A* 109(15):5687–5692.
35. Murakami S, Nakashima R, Yamashita E, Matsumoto T, Yamaguchi A (2006) Crystal structures of a multidrug transporter reveal a functionally rotating mechanism. *Nature* 443(7108):173–179.
36. Nakashima R, et al. (2013) Structural basis for the inhibition of bacterial multidrug exporters. *Nature* 500(7460):102–106.
37. Chen VB, et al. (2010) MolProbity: All-atom structure validation for macromolecular crystallography. *Acta Crystallogr Sect D Biol Crystallogr* 66(1):12–21.
38. DeWitt S, Adelberg E (1962) The occurrence of a genetic transposition in a strain of Escherichia coli. *Genetics* 47(May):577–685.